waveform approach for complete moment tensor inversion and stress estimation

F. Song, M. N. Toksöz & J. Li
Earth Resources Laboratory, MIT, Cambridge, USA

ABSTRACT: Downhole microseismics has gained in popularity in recent years as a way to characterize hydraulic fracturing sources and to estimate in-situ stress state. Conventional approaches only utilize part of the information contained in the microseismic waveforms such as the P/S amplitude ratio and/or P first motion polarity to determine the microearthquake focal mechanisms and infer stress state. Thus, additional constraints like double-couple assumption must be made to stabilize the inversion for conventional methods. The situation becomes even worse for downhole monitoring where only limited azimuthal coverage is available. In this study, we have developed a full-waveform based approach to invert for complete moment tensor. We use the discrete wavenumber integration approach as the fast forward modeling tool to calculate the synthetic waveforms for one-dimensional layered velocity models. By matching full three-component waveforms across the array, a stable moment tensor solution can be obtained without imposing additional constraints. We also derive the source radius from the far-field displacement spectrum with the Madariaga's model and determine the stress drop afterwards. We test our method on a downhole microseismic dataset from hydraulic fracturing treatments in East Texas. The result indicates the existence of the isotropic component in some events. A clear difference is observed that non-double-couple events tend to have smaller stress drops, which is consistent with other studies. The derived fracture plane direction also agrees with that derived from multiple event location.

1 INTRODUCTION

Microseismic downhole monitoring is a valuable tool for mapping the fractures and evaluating the effectiveness of hydraulic fracturing. The locations of microseismic events, with sufficient resolution, provide information on fracture geometry and properties (Warpinski et al. 1998, Phillips et al. 2002).

However, additional information besides location is contained in the microseismic waveforms. For example, seismic moment tensor has gained more and more interests recently in terms of understanding the microseismic source mechanisms and stress state (Nolen-Hoeksema & Ruff 2001, Baig & Urbancic 2010). Although moment tensor inversion has been applied in downhole hydraulic fracturing monitoring, most of them rely only on P- and S- wave amplitudes and/or P-wave first motion polarities. Due to the limited usage of waveform information, these approaches normally either require multiple monitoring wells from different azimuths or make double-couple source assumptions in order to stabilize the inversion (Vavrycuk 2007, Baig & Urbancic 2010). In most cases of hydraulic fracturing, data are available from only one monitoring well. Given this limitation, the following questions arise: 1) can we invert complete moment tensor with data from one single well? 2) how can we stabilize the inversion without making the assumption of double-couple sources?

In this paper, we propose a full-waveform approach for moment tensor inversion with one single monitoring well. It uses the discrete wavenumber integration method to calculate the full elastic wavefield in the layered medium. By matching full waveforms across the geophone array, we show that the moment tensor inversion can be stabilized so that the complete moment tensor solution can be retrieved from an array of three-component geophones in a single borehole. In this paper, we begin by introducing the full-waveform based moment tensor inversion approach and testing the method with synthetic data to extract seismic moment, fracture orientation, and the isotropic component part of the moment tensor. Then we describe the application to a field dataset from East Texas. We invert the full seismic moment tensor and derive stress drop from the far-field displacement spectrum based on Madariaga's model (Madariaga 1976).

2 METHODOLOGY

2.1 *Full waveform based moment tensor inversion*

The moment tensor of microseismic events can be represented by a 3 by 3 symmetric matrix m_{jk} (Aki & Richards 2002). To improve the inversion with a single borehole coverage, we use all phases that are embedded in the full waveform data. Our approach starts from full elastic waveform modeling in the layered medium with discrete wavenumber integration method (DWN; Bouchon 2003). The i-th component (North, East, Down) of the observed waveform at geophone n is modeled as:

$$v_i\left(x_r^n, x_s, t\right) = \sum_{j=1}^{3}\sum_{k=1}^{3} m_{jk} G_{ij,k}\left(x_r^n, x_s, t\right) \otimes s(t) \quad (1)$$

where $G_{ij,k}\left(x_r^n, x_s, t\right)$ is the i-th component of the Green's function at geophone x_r^n from a point moment tensor source m_{jk} at x_s, $s(t)$ is the source time function. In this study, a smooth ramp function is used as $s(t)$.

The misfit function for inverting moment tensor matrix m_{jk} is defined by:

$$\Delta(m_{jk}) = \sum_{n=1}^{N}\sum_{i=1}^{3}\int_0^{T_n}\left(d_i\left(x_r^n, x_s, t\right) - v_i\left(x_r^n, x_s, t\right)\right)^2 dt \quad (2)$$

where $d_i\left(x_r^n, x_s, t\right)$ is the observed data, while $v_i\left(x_r^n, x_s, t\right)$ is the synthetic data as described in Equation 1. T_n is the duration of observed waveforms at geophone n. In this study we choose T_n to include both P and S wave trains and is constant for all geophones. Time 0 is the origin time, which is obtained by grid-search around its initial estimate within the dominant signal period. The initial estimate of the origin time can be found by cross-correlating the synthetic and observed waveforms. To further stabilize the inversion, we band-pass filter both synthetic data and observed data to the signal frequency band, which we select [200, 900] Hz in this study. The moment tensor is solved by minimizing the misfit function in Equation 2 as:

$$M_i(x_s) = \left(A^{-1}\right)_{ij}(x_s) D_j(x_s) \quad (3)$$

Here M_i is the i-th component of six independent moment tensor elements: $M_1 = m_{11}$, $M_2 = m_{22}$, $M_3 = m_{33}$, $M_4 = m_{12}$, $M_5 = m_{13}$, $M_6 = m_{23}$, while D_j has six independent elements:

$$D_j(x_s) = \sum_{n=1}^{N}\sum_{k=1}^{3}\int_0^{T_n} g_{kj}\left(x_r^n, x_s, t\right) d_k(x_r^n, x_s, t)dt \quad (4)$$

where j = 1, 2, 3…6 and g_{kj} corresponds to one of the six elementary seismograms and each is defined by:

$$g_{kj}(x_r^n, x_s, t) = G_{kj,\,j}(x_r^n, x_s, t) \otimes s(t),\ j = 1,2,3 \quad (5)$$

$$g_{k4}(x_r^n, x_s, t) = [G_{k1,2} + G_{k2,1}] \otimes s(t) \quad (6)$$

$$g_{k5}(x_r^n, x_s, t) = [G_{k1,3} + G_{k3,1}] \otimes s(t) \quad (7)$$

$$g_{k6}(x_r^n, x_s, t) = [G_{k2,3} + G_{k3,2}] \otimes s(t) \quad (8)$$

Finally A is a 6*6 matrix with elements:

$$A_{ij}(x_s) = \sum_{n=1}^{N}\sum_{k=1}^{3}\int_0^{T_n} g_{kj}\left(x_r^n, x_s, t\right) g_{ki}(x_r^n, x_s, t)dt \quad (9)$$

Once we obtain the full moment tensor matrix m_{jk}, we can obtain seismic moment as:

$$M_0 = \max\left|\lambda_i\right| \quad (10)$$

where λ_i is the eigenvalue of moment tensor matrix. The moment magnitude is defined as:

$$M_w = \frac{2}{3}\log_{10}(M_0) - 6.067 \quad (11)$$

where M_0 is the seismic moment in N*m. The full moment tensor matrix is further decomposed into three parts: isotropic (ISO) component, compensated linear vector dipole (CLVD) component and double-couple (DC) component (Vavrycuk 2001). The fracture strike is then derived from the DC component (Jost & Hermann 1989). The ISO percentage is obtained by:

$$c^{ISO} = \frac{1}{3}\frac{tr(m_{jk})}{M_0}100\% \quad (12)$$

2.2 *Stress drop estimation*

According to (Madariaga 1976), the radius of a circular source can be estimated from:

$$r_0 = \frac{1.32 V_s}{2\pi f_c} \quad (13)$$

where f_c is the corner frequency derived from S-wave displacement spectrum. Stress drop, defined as the average difference between the initial and final stress levels over the fault plane, is obtained from:

$$\Delta\sigma = \frac{7}{16}\frac{M_0}{r_0^3} \quad (14)$$

where M_0 is the seismic moment determined by full moment tensor inversion as shown in Equation 10.

3 SYNTHETIC STUDY

3.1 *Full waveform fitting and seismic moment tensor inversion*

For the synthetic study, we use DWN to generate clean data. We add 10% Gaussian noise to form the synthetic data. Figure 1 shows the 1D velocity model used for the synthetic study, which is identical to the following field study.

The red curve in Figure 2 shows the synthetic three-component data for a double-couple source (strike: 85 degrees, dip: 75 degrees, rake: 0 degree) at a vertical depth of 3975.3 m and 64.8 m north, 77.3 m west away from the six-geophone array in the vertical monitoring well. The inverted data is shown in blue for each plot. We see a pretty good agreement between synthetic data and inverted data. Besides fitting the P- and S-wave, we also see a good fit for P & S converted wave. This additional waveform information helps constrain the inversion and lower the condition number of the matrix A. This is also the reason why we can invert for full moment tensor from one vertical geophone array without making additional source assumptions. The inverted moment tensor gives a fracture plane with strike of 84.9 degrees, dip of 74.5 degrees, and rake of -0.6 degrees, which is pretty close to the true value especially the strike value. This shows the validity of our approach in extracting fracture geometry information, among which strike information is the most interesting.

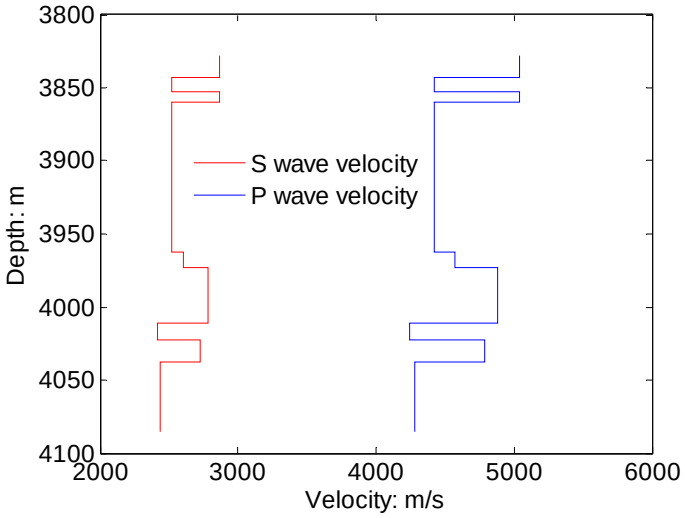

Figure 1. One-dimensional P- and S-wave velocity model for both synthetic study and field study, which is derived from well logging data.

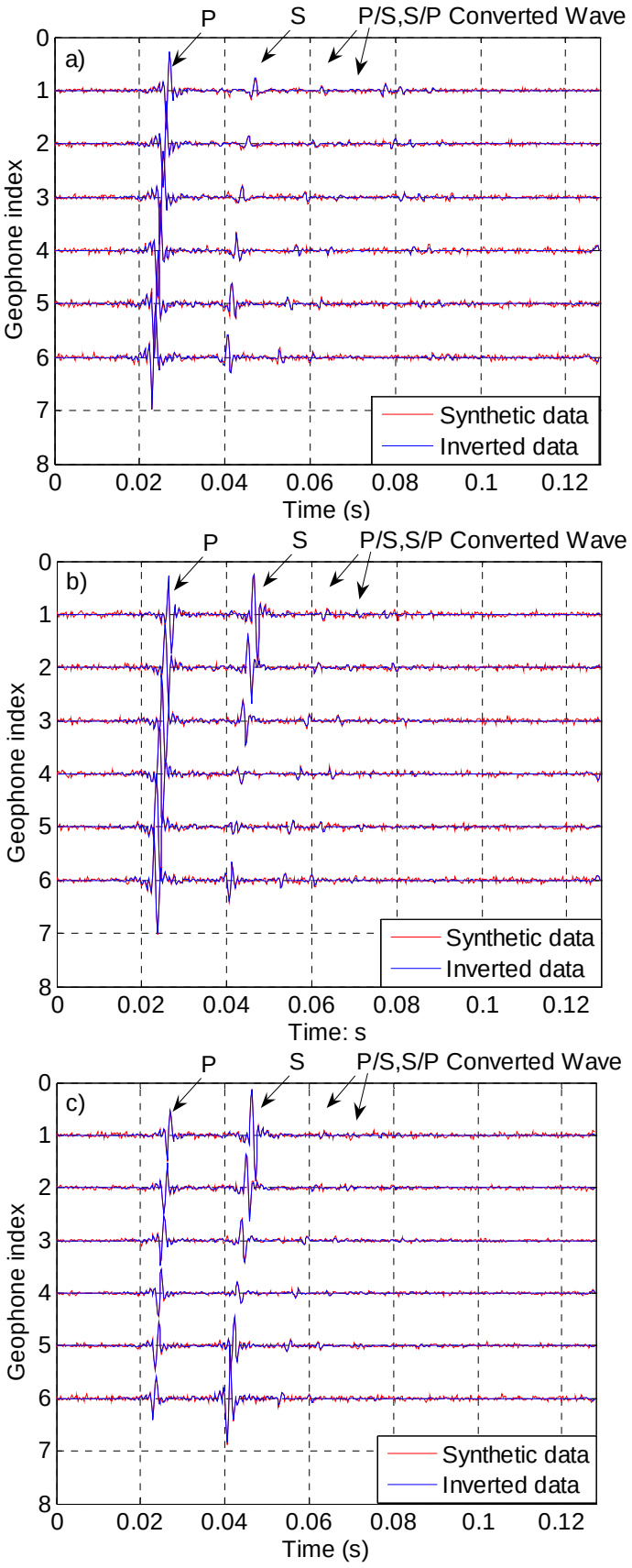

Figure 2. Three-component velocity waveform fitting: a) North component, b) East component, c) Down component. The red curve shows the synthetic data with 10% Gaussian noise, while the blue curve gives the fitted data from moment tensor inversion.

3.2 *Seismic moment estimate*

To evaluate the accuracy of the seismic moment estimated by our method, we conduct the Monte-Carlo simulation. In this experiment, we fix the source location at (N,E,D) = (64.8, 77.3, 3975.3) m and a source mechanism of (strike, dip, rake) = (85, 75, 0) degrees. We vary the seismic moment from 10^3 N·m to 10^8 N·m. For different seismic moment values, different realizations of 10% Gaussian noise are added to the synthetic data to study the statistical properties of the seismic moment estimator. For each seismic moment value, a full-waveform moment tensor inversion as described above is performed to retrieve the seismic moment.

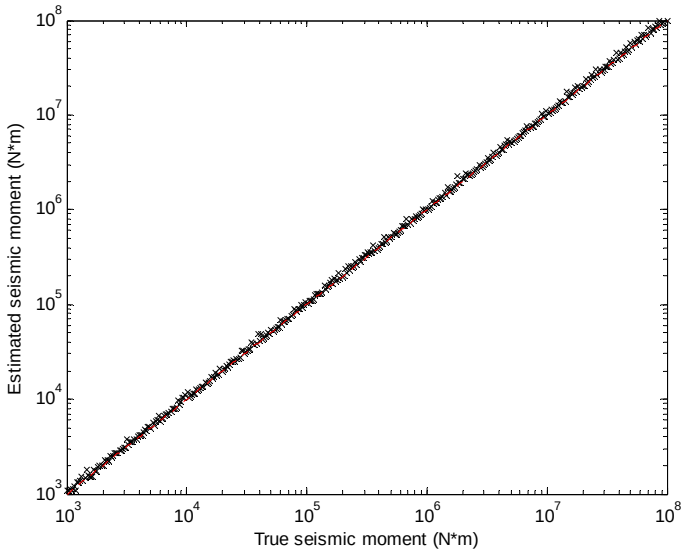

Figure 3. Comparison of true seismic moment and estimated seismic moment.

Figure 3 gives the comparison between true seismic moment used to generate synthetic data and the estimated seismic moment by full moment tensor inversion. The estimated seismic moment values agree well with the true seismic moment values. The mean error is around 3.9%, while the standard deviation is about 5.2%. This means that the true values of M_0 are within the confidence region of the estimated M_0 under additive Gaussian noise, which is consistent with previous study (Patton & Aki 1979). The non-zero bias comes from two parts: 1) the errors propagated into the moment tensor inversion solution due to the additive data noise, which is well bounded by the illness of matrix A; 2) the numerical errors from the eigenvalue decomposition as described in Equation 10. In summary, for a broad range of seismic moment values, our method gives a good estimate.

3.3 *Strike estimate*

A similar Monte-Carlo simulation has been conducted to assess the performance of strike estimator. For this test, we test two source mechanisms. One is the pure double-couple mechanism while the other is a 60% double-couple component with a 40% isotropic component. For both scenarios, the dip and rake value is set to be 75 and 0 degrees. We also fix the source location same as in Section 3.2 and use a constant seismic moment of $5*10^4$ N·m. The strike value is changed from 0 to 360 degrees. For each strike value, a forward modeling with 10% additive Gaussian noise is conducted and a full-waveform moment tensor inversion is performed afterwards to invert for the full moment tensor and retrieve the strike.

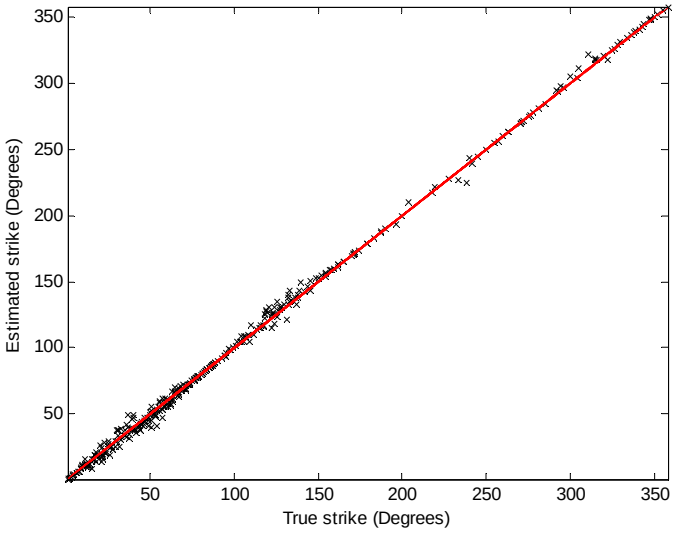

Figure 4. Comparison of true strike and estimated strike (pure DC source).

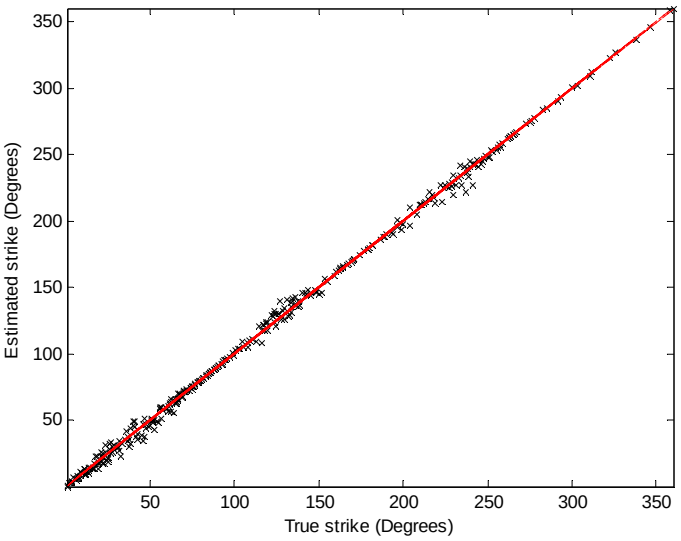

Figure 5. Comparison of true strike and estimated strike (source: 60% DC component + 40% ISO component).

The estimated strike value is plotted against the the true strike value for both cases in Figures 4 and

5. The estimated strike is in good agreement with the true strike. The estimated strike has a mean error of -0.1 degrees from the true strike for the pure DC source, while the mean error increases to 0.3 degrees for the isotropic plus double-couple source. The increased error in strike is due to the decreased deviatoric part of the seismic moment tensor, from which the strike is defined.

3.4 *Isotropic component percentage estimate*

The isotropic component percentage defined in Equation 12 provides a good indicator of fracture volumetric strain. It gives some idea about fracture opening and closure. As discussed in Section 3.3, it also indicates the uncertainty of strike estimates to some degree. The higher the isotropic component percentage is, the less accurate the strike estimate is.

In this simulation, we change the relative percentage between DC component and the ISO component and fix the seismic moment to be $5*10^4$ N·m. All other parameters are kept the same as Section 3.2. Figure 6 represents the comparison between true isotropic percentage and the estimated isotropic percentage. The estimated ISO percentage generally agrees well with the true ISO percentage. There is some scattering for the estimates due to 10% Gaussian noise. The mean error is around -0.2%, while the standard deviation approaches 2.6%. This means the true isotropic percentage value falls into the confidence region of the estimated isotropic percentage, although the maximum absolute error is close to 8%.

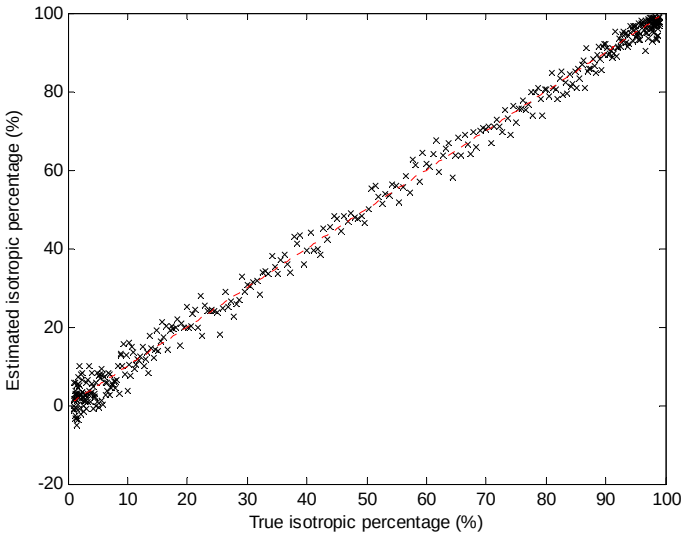

Figure 6. Comparison of true isotropic percentage and estimated isotropic percentage.

4 FIELD STUDY

4.1 *Field setup*

A microseismic survey was conducted during the hydraulic fracturing treatment of the Bonner sands in the Bossier play at a depth approximately from 3956 m (12980 ft) to 3981 m (13060 ft). The microseismic data was collected using a twelve-level, three-component geophone array deployed in the vertical monitoring well at a depth from 3874 m (12710 ft) to 3944 m (12940 ft). The treatment well is approximately 151 m (495 ft) away from the monitoring well. The recorded data was analyzed and located for hydraulic fracturing mapping as outlined by Griffin et al. (2003), and Sharma et al. (2004). The velocity model used for location is shown in Figure 1. In this study, we test our method on several located microseismic events to invert for the complete moment tensor and estimate the stress drop from the full waveforms. The microseismic data from the lower six geophones at a depth from 3912 m (12835 ft) to 3944 m (12940 ft) are selected due to their higher signal-to-noise ratios (SNRs). Figure 7 shows the horizontal plane view of the monitoring well at the origin and seven selected microseismic events, which shows a fracture plane mostly along W-E direction. This has been demonstrated in the paper by Sharma et al. (2004).

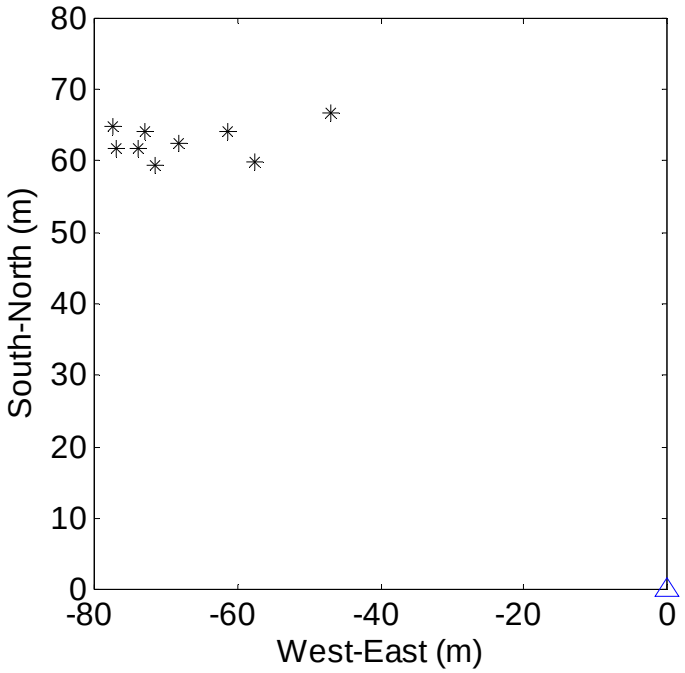

Figure 7. Horizontal plane view of selected microseismic events.

In next section, we will show the results from full waveform moment tensor inversion and stress drop estimation. We will use one event, named event 1, to demonstrate our procedure. Then we will present and discuss the results for all seven chosen events.

4.2 *Seismic moment tensor inversion and stress drop estimation*

As described in section 2, we firstly invert for complete moment tensor from full waveforms and extract three important parameters: 1) seismic moment, 2) strike, and 3) isotropic component percentage. Figures 8 a) and b) give the waveform fitting of event 1 between synthetic data and observed data for the north and east component separately. Here only two horizontal components are used in the inversion, because the vertical component has a much poorer SNR due to the poor clamping to the formation. A good agreement of dominant P and S wave trains is seen in both Figures 8 a) and b). The un-modeled wave packages are probably due to the scattering from un-modeled lateral heterogeneity.

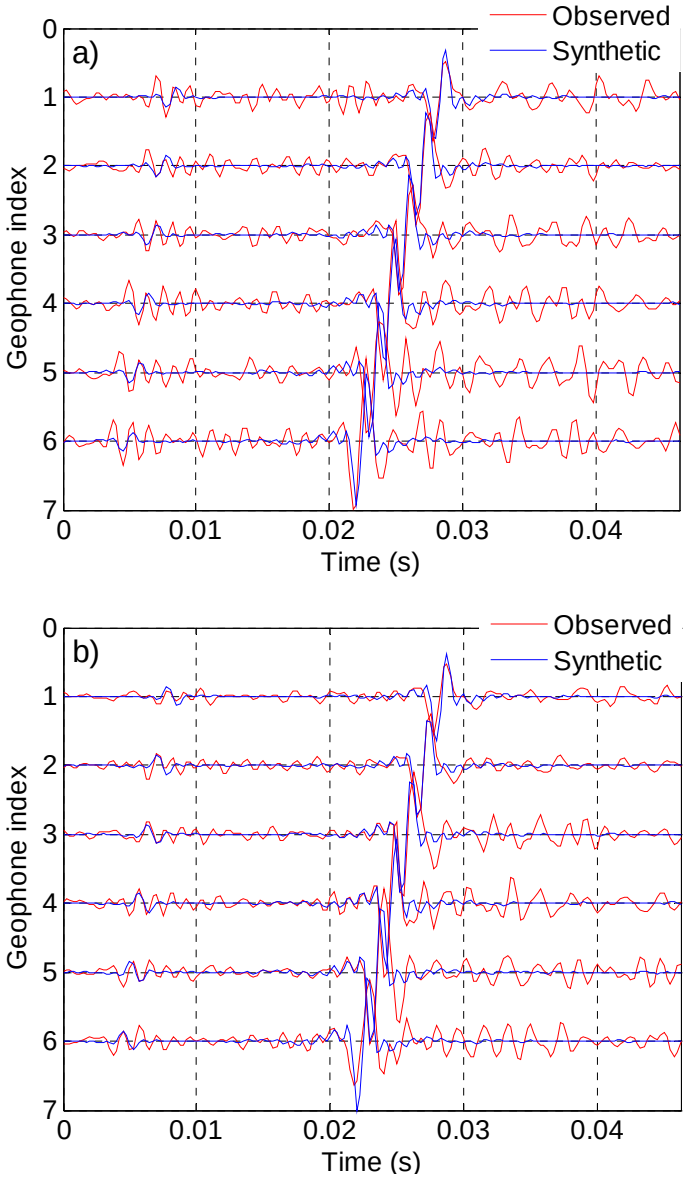

Figure 8. Comparison between synthetic data and observed data for event 1: a) North component, b) East component.

The estimated seismic moment, strike and the isotropic percentage for event 1 are listed in Table 1. We see a negative isotropic component for event 1, which implies a contribution from implosion. This possibly corresponds to some degree of fracture closure. The seismic moment for event 1 is around $6.1*10^4$ N·m, suggesting a moment magnitude around -2.87. The strike estimated from the deviatoric component gives the values for the fracture plane and the auxiliary plane. It is hard to tell the fracture plane from one single event. The strike values determined from moment tensor inversion for all seven events are listed in Table 1. Compared to the fracture orientation reported in the paper by Sharma et al. (2004), the first set of strike values agrees well with their result of $N87^0E$ derived from multiple event location and gives the fracture plane strike. The scattering around $N87^0E$ possibly comes from three factors: 1) velocity model inaccuracy, 2) location errors, and 3) noise contamination as shown in Section 3.3.

Table 1. Results of source parameter determinations.

Event	M_0	M_w	Strike	
	10^4 N·m		Degrees (East of North)	
1*	6.1	-2.87	102	12
2*	2.1	-3.17	80	207
3*	8.1	-2.79	73	196
4*	45	-2.29	139	39
5	5.3	-2.91	75	197
6	7.5	-2.81	95	211
7	4.4	-2.96	82	203

Table 1 continued.

Event	M_w	f_c	r_0	$\Delta\sigma$	ISO percentage
		Hz	m	Kpa	%
1*	-2.87	481	1.2	14.9	-26
2*	-3.17	561	1.0	8.3	29
3*	-2.79	547	1.1	29.2	31
4*	-2.29	564	1.0	178.0	30
5	-2.91	714	0.8	42.7	11
6	-2.81	736	0.8	65.8	-10
7	-2.96	744	0.8	39.6	-4

To estimate the stress drop, Madariaga's (1976) model is adopted to estimate the source radius from the S-wave corner frequency. The recorded voltage data is converted to displacement considering the geophone response (Warpinski 2009). The spectral analysis is then applied to the converted S-wave displacement data. For event 1, Figure 9 shows the S-wave displacement spectrum and the best-fit curve determined from the kinematic model defined by the following equation:

$$U(f) = \frac{\Omega_0 \cdot e^{-\pi f R / V_S Q_S}}{1 + (f/f_c)^2} \tag{15}$$

where R is the source-receiver distance, Qs = 100 is the S-wave quality factor. In the present case of event 1, average values of 2605 m/s and 112 m are accepted for the S-wave velocity and the source-receiver distance separately. A simple nonlinear-least square inversion is deployed to estimate corner frequency f_c (Talebi & Boone 1998). Source radius r_0 is then derived from f_c according to Equation 13. The stress drop is finally determined from previously obtained source radius and seismic moment by Equation 14. The stress drop values for all seven events are listed in Table 1. A clear difference is observed between estimates of stress release parameters for the two types of events as those events having a significant isotropic component percentage (marked as * in Table 1) tend to have smaller stress drops compared to deviatoric type events of a similar magnitude range. This is consistent with previous studies of injection-induced microseismicity in oil fields (Talebi & Boone 1998). The possible explanation is that the source areas associated with events having significant isotropic components are more likely to have weaker shear strengths, and thus smaller stress drops.

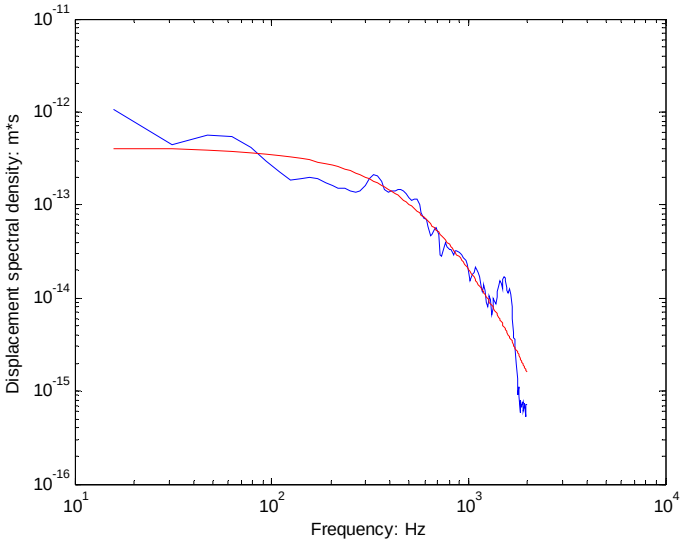

Figure 9. S-wave displacement spectrum: observed (blue) and model fitted (red).

5 CONCLUSIONS

In this paper, we developed a full-waveform based moment tensor inversion approach for hydraulic fracturing monitoring using one single monitoring well. By exploring full waveform information in a one-dimensional layered medium instead of using only P/S amplitude ratio and/or P first motion polarity, we have demonstrated that the complete moment tensor inversion can be stabilized without making additional double-couple source assumptions. By synthetic and field test, we have shown that the strike, isotropic component and stress drop can be reliably derived from this full waveform analysis approach assuming a certain source model. Synthetic tests also indicate that additive Gaussian noises do not pose difficulties for recovering reliable estimates of the moment tensor. Field data examples show the existence of both deviatoric type events and isotropic type events. In both cases, the derived strike values are in good agreement with the fracture azimuth determined from multiple event locations. However, stress drop studies indicate that isotropic type microseismic events tend to have smaller stress drops compared to deviatoric type events of a similar magnitude range. Errors in source parameter estimates may come from the inaccuracies in source locations and velocity models. Future work includes further refinement over source locations and velocity models. This full-waveform approach has a great potential to improve the source properties study in the situations where only a single monitoring well is available.

Acknowledgements

The authors would like to thank Pinnacle - A Halliburton Service for providing the data and for funding this research. We are grateful to Dr. Norm Warpinski, Dr. Jing Du, Dr. Erkan Ay and Dr. Qinggang Ma from Halliburton Energy Services Company, Dr. Michael Fehler and Dr. William Rodi from MIT for their helpful suggestions. We thank Halliburton Energy Services Company and Anadarko Petroleum Corporation for permission to publish this work.

REFERENCES

Baig, A. & Urbancic, T. 2010. Microseismic moment tensors: A path to understanding frac growth. *The Leading Edge* 29(3): 320-324.

Bouchon, M. 2003. A review of the discrete wavenumber method. *Pure and Applied Geophysics* 160: 445-465.

Griffin, L.G., Sullivan, R.B., Wolhart, S.L., Waltman, C.K., Wright, C.A., Weijers, L. & Warpinski, N.R. 2003. Hydraulic Fracture Mapping of the High-Temperature, High-Pressure Bossier Sands in East Texas. *SPE Annual Technical Conference and Exhibition, Denver, 5-8 October 2003*: Paper 84489.

Jost, M.L. & Herrmann, R.B. 1989. A student's guide to and review of moment tensors. *Seismological Research Letters* 60(2):37-57.

Madariaga R. 1976. Dynamics of an Expanding Circular Fault. *Bulletin of the Seismological Society of America* 66:639–666.

Nolen-Hoeksema, R.C. & Ruff, L.J. 2001. Moment tensor inversion of microseisms from the B-sand propped hydrofracture, M-site, Colorado. *Tectonophysics* 336(1-4): 163-181.

Patton, H. & Aki, K. 1979. Bias in the estimate of seismic moment tensor by the linear inversion method. *Geophysical Journal of the Royal Astronomical Society* 59(3): 479-495.

Phillips, W., Rutledge, J. & House, L. 2002. Induced microearthquake patterns in hydrocarbon and geothermal reservoirs: six case studies. *Pure and Applied Geophysics* 159: 345-369.

Sharma, M.M., Gadde, P.B., Sullivan, R., Sigal, R., Fielder, R., Copeland, D., Griffin, L., and Weijers, L. 2004. Slick Water and Hybrid Fracs in the Bossier: Some Lessons Learnt. *SPE Annual Technical Conference and Exhibition, Houston, 26–29 September 2004*: Paper 89876.

Talebi, S. & Boone, T.J. 1998. Source parameters of injection-induced microseismicity. *Pure and Applied Geophysics* 153:113-130.

Vavrycuk, V. 2007. On the retrieval of moment tensors from borehole data. *Geophysical Prospecting* 55:381-391.

Vavrycuk, V. 2001. Inversion for parameters of tensile earthquakes. *Journal of Geophysical Research* 106(B8):16339-16355.

Warpinski, N.R 2009. Microseismic monitoring: inside and out. *Journal of Petroleum Technology* 61: 80-85.

Warpinski, N.R., Branagan, P.T., Wolhart, S.L. & Uhl, J.E. 1998. Mapping hydraulic fracture growth and geometry using microseismic events detected by a wireline retrievable accelerometer array. *SPE Gas Tech. Symp., Calgary, 15-18 March 1998*: Paper 40014.